Energy level alignment at the interfaces in a multilayer organic light-emitting diode structure

S. Olthof,* R. Meerheim, M. Schober, and K. Leo
Institut für Angewandte Photophysik, Technische Universität Dresden, D-01062 Dresden, Germany
(Received 2 March 2009; revised manuscript received 4 May 2009; published 11 June 2009)

We use photoelectron spectroscopy to study the electronic structure and energy level alignment throughout an organic light-emitting diode. The structure under investigation is a state-of-the-art long-living red phosphorescent device composed of doped charge-injection layers, charge-blocking layers, and an emission layer. By consecutively building up the whole device, the key parameters of every interface are measured. Our results show that the doped layers have a significant influence on the device energetics, especially in controlling the built-in potential, and that there are mostly only small dipoles present at the interfaces of the intrinsic organic layers.

DOI: 10.1103/PhysRevB.79.245308 PACS number(s): 79.60.Fr, 85.60.Jb

I. INTRODUCTION

Current highly efficient organic light-emitting diodes (OLEDs) consist of a large number of different organic layers such as doped injection layers, blocking layers, and active emitting layer.[1] With rising complexity of the device stack, the interfaces between these layers become increasingly important for the OLED performance. For simplicity, vacuum-level alignment is usually assumed so that the independently measured highest occupied molecular orbital (HOMO) and lowest unoccupied molecular orbital (LUMO) can be used to obtain the energy diagram. However, it is well known from detailed spectroscopic studies on model systems that interface dipoles originating from effects such as polarization, chemical reactions, and bond formation very often change the simple picture of vacuum alignment.[2] In our devices, we use doped layers to increase the carrier density, facilitate carrier injection, and ensure Ohmic contact behavior; therefore the alignment is affected by the level bending and the resulting depletion layer.[3] These effects can lead to deviations as large as 2 eV from the commonly assumed vacuum-level alignment. To obtain deeper insight into simulation and optimization of a full OLED device, it is therefore necessary to measure the energy alignment at all metal/organic and organic/organic interfaces. This can be performed, e.g., by ultraviolet photoelectron spectroscopy (UPS) and x-ray photoelectron spectroscopy (XPS). Various studies of organic/organic[4,5] and metal/organic[6] interfaces can be found in literature. However, to understand the alignment in a complete device, it is not sufficient to look at individual interfaces since the choice of the electrode material,[7] pinning effects of organic layers,[8] polar-bond orientation,[9] or doping-induced level bending can influence the energetic position of the following layers and thereby the interface formation.

In this paper, we present interface resolved studies of an incrementally built complete OLED structure by UPS and XPS. We show that significant interface dipoles and a built-in potential are present in such a device structure. Also, we show that, in particular, doped layers can determine the energetic positions of several subsequent layers.

For our studies, we choose the structure of a long living and highly efficient red phosphorescent device.[10] In this stack, an indium tin oxide (ITO) anode is contacted by a hole-injection layer consisting of *N*,*N*,*N*′,*N*′-tetrakis(4-methoxyphenyl)-benzidine (MeO-TPD) doped with 4 mol % of 2,3,5,6-tetrafluoro-7,7,8,8-tetracyanoquinodimethane (F4-TCNQ) and an electron-blocking layer of *N*,*N*′-di(naphthalen-1-yl)-*N*,*N*′-diphenyl-benzidine (α-NPD). This is followed by a light-emitting layer composed of α-NPD coevaporated with 10 wt % of the phosphorescent red emitter iridium(III) bis(2-methyldibenzo[f,h]quinoxaline)(acetylacetonate) [$Ir(MDQ)_2acac$] and a hole-blocking layer of 4,7-diphenyl-1,10-phenanthroline (BPhen). Finally, there is an electron-injection layer of BPhen doped by cesium and a silver top contact.

II. EXPERIMENT

Measurements are performed with a Phoibos100 system (Specs, Berlin, Germany) under ultrahigh vacuum (UHV) with a base pressure of 1×10^{-10} mbar. For UPS measurements, the He I line (21.22 eV) from a discharge lamp with an energy resolution of 130 meV and for XPS an Al $K\alpha$ x-ray source (1486.6 eV) with a resolution of 400 meV are used. The experimental error of both methods can be estimated from the reproducibility achieved in separate measurements and is below 50 meV. The UHV evaporation tool with a base pressure of $\leq1\times10^{-8}$ mbar for the deposition of the organic layers is directly connected to the measurement chamber and different chambers for *n*- and *p*-type doping as well as for intrinsic layers can be used to avoid cross contamination.

The OLED samples for the characterization of the current-voltage curves were prepared in a different single-chamber UHV system (Kurt J. Lesker Co. Ltd., Hastings, UK) at a base pressure of 1×10^{-8} mbar. Here it is possible to fabricate devices with different structures on the same sample ensuring equal evaporation conditions for a high comparability. After preparation, the devices are encapsulated with cavity glass lids by an epoxy glue under the nitrogen atmosphere of a glovebox that is directly attached to the vacuum system.

The organic materials MeO-TPD and α-NPD (both Sensient, Wolfen, Germany) two times sublimated, BPhen (Ald-

 ©2009 The American Physical Society

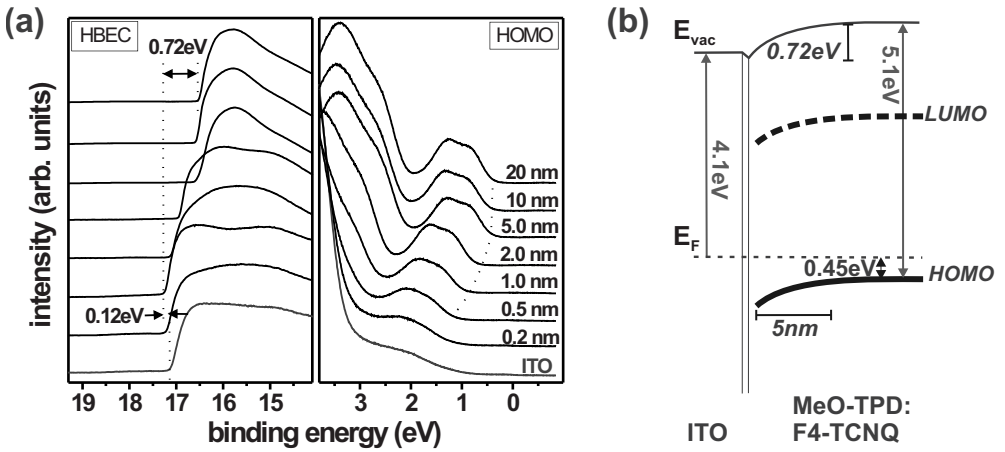

FIG. 1. Interface between ITO and MeO-TPD doped with 4 mol % of F4-TCNQ. (a) Development of the HBEC and HOMO region of the UPS He I spectra as a function of increasing thickness of the organic layer. The dotted lines mark the change in vacuum level and HOMO position. (b) Resulting schematic energy level diagram.

rich, Munich, Germany) two times sublimated, and F4-TCNQ and $Ir(MDQ)_2acac$ (both TCI, Zwijndrecht, Belgium) one time sublimated were deposited at room temperature from heated crucibles. Cesium was purchased from Saes (Milan, Italy) and is evaporated out of an alloy. Doping is achieved by coevaporating host and dopand while the evaporation rates are controlled independently by two quartz crystals. As substrate, either sputter-treated ITO (Thin Film Devices, Inc., Anaheim, USA) or sputter-cleaned silver foil (99.995%, MaTecK, Juelich, Germany) is used. The metal/organic and organic/organic interfaces are built incrementally in the same order as in the OLED device and the measurement steps in each layer range in thickness from 2 Å up to 20 nm. For each step, the high-binding energy cutoff (HBEC), the hole-injection barrier (HIB), and characteristic core-level peaks are measured. Several UPS measurements are taken successively to ensure that the sample shows no sign of charging.

III. RESULTS AND DISCUSSION

The first interface investigated is the one from the anode ITO to the hole-injection layer MeO-TPD *p* doped with 4 mol % of F4-TCNQ. Before measurement, the ITO is sputter cleaned using argon to remove residual carbon. This is necessary since ITO commonly shows degradation under UV excitation due to a reaction with surface contaminations.[11] After the treatment, the anode shows a work function (W_f) of 4.1 eV. On top of this, the organic semiconductor is deposited in steps to observe interface and level-bending effects. The development of the HBEC and HOMO region of the UPS spectra taken at different layer thicknesses is shown in Fig. 1(a). Here, as in all following spectra, the binding-energy scale is in reference to the Fermi edge of the anode and the curves are vertically shifted for clarity.

Within the first 0.5 nm, an interface dipole of −120 meV is observed in the vacuum level that is followed by an upward bending of 720 meV. The HOMO of the MeO-TPD can be clearly observed after 1 nm deposition and shows the same bending behavior as the vacuum level. After a depletion region of 5 nm, the energy levels saturate, resulting in a HIB of 0.45 eV and the ionization potential (IP) of MeO-TPD is 5.1 eV. The resulting energy diagram for this interface is shown in Fig. 1(b) where a HOMO-LUMO gap of 3.2 ± 0.3 eV is assumed, as determined from optical-

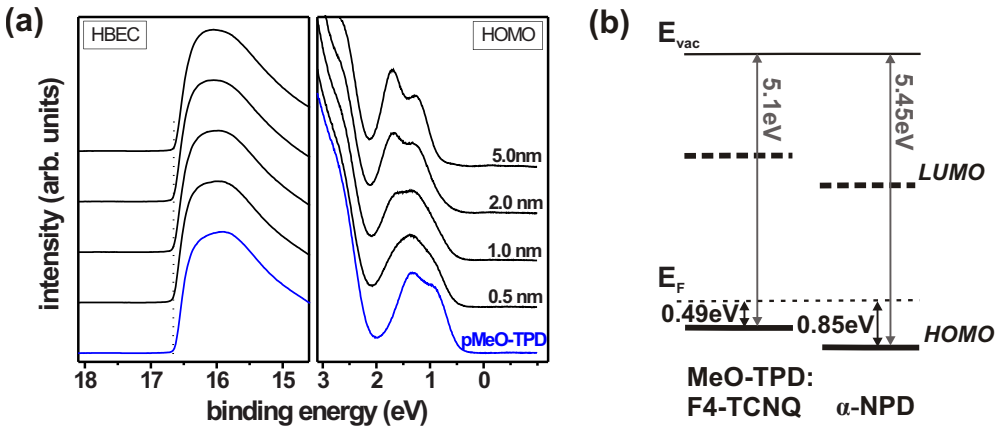

FIG. 2. (Color online) Interface between doped MeO-TPD and α-NPD. (a) Development of the HBEC and HOMO region of the UPS He I spectra as a function of increasing thickness of the α-NPD layer. The dotted vertical line marks the HBEC position. (b) Resulting schematic energy level diagram.

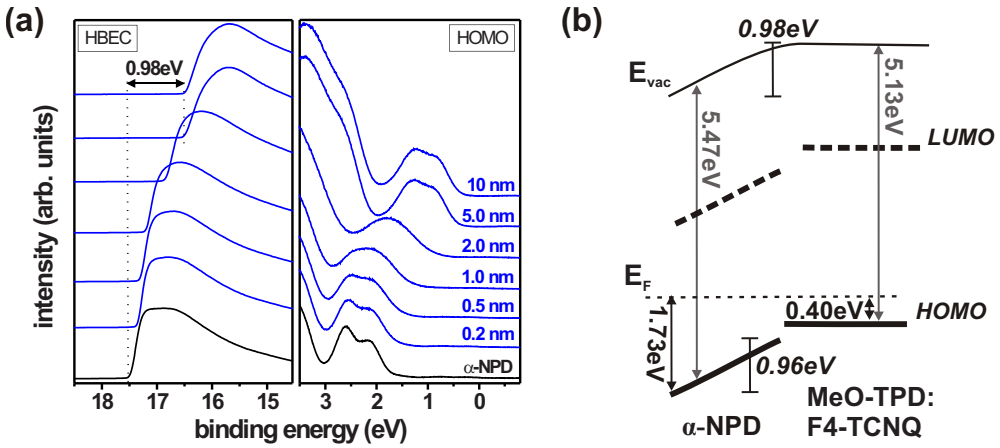

FIG. 3. (Color online) Interface between α-NPD and doped MeO-TPD. (a) Development of the HBEC and HOMO region of the UPS He I spectra as a function of increasing thickness of the doped MeO-TPD layer. The dotted vertical line marks the change in the position of the HBEC. (b) Resulting schematic energy level diagram.

absorption edge measurements.[12] The larger error margin of this value is due to the unknown exciton binding energy that is estimated to be 0.3 eV.[13] Since ITO is less reproducible and more difficult to handle compared to a metal foil, the same experiment was repeated using a sputter-cleaned silver foil with a W_f of 4.3 eV. Again after 5 nm the level bending is completed and this contact results in the same energetic position of the thick p-MeO-TPD layer (data not shown). The equivalence of these substrates gets apparent when comparing the ionization potential and HIB of the 20 nm p-MeO-TPD layer on ITO of Fig. 1 and the 6 nm p-MeO-TPD layer on silver of Fig. 2. As the values coincide one can assume equal growth modes in both cases.[14] Therefore, for all the following measurements a silver foil is used as a substrate.

For the investigation of the interface between MeO-TPD:F4-TCNQ and the intrinsic α-NPD blocking layer, a layer of doped MeO-TPD (6 nm) is prepared on a silver foil and subsequently α-NPD is evaporated. No dipole is observed at the interface as can be seen from the constant HBEC in Fig. 2(a), so there is vacuum-level alignment between the two layers. The IP of the 5-nm-thick α-NPD layer is 5.45 eV and the HIB is 0.85 eV as is shown in Fig. 2(b); here a transport gap of 3.1 eV is assumed for α-NPD that was measured by inverse photoelectron spectroscopy.[4]

Using this interface, one can nicely show the strong influence of the doped layer on the energetic alignment within the OLED device. If the deposition order of the two layers is reversed as shown in Fig. 3 and α-NPD is directly put on silver, the HIB is 1.73 eV, about 1 eV larger compared to the same layer deposited on the doped MeO-TPD. If then the MeO-TPD:F4-TCNQ layer is deposited on top, a shift of 980 meV happens in the vacuum level as the HOMO of the doped layer shifts close to the Fermi energy again. Fitting the HOMO regions of the different thicknesses with peaks for α-NPD and MeO-TPD shows that the HOMO of α-NPD gets pulled up by 960 meV due to the contact with the doped layer. This shift is due to the electrostatic field introduced between metal and ionized dopands.

On a further sample, the interface between intrinsic α-NPD and the active layer where α-NPD is coevaporated with 10 wt % of the phosphorescent emitter $Ir(MDQ)_2acac$

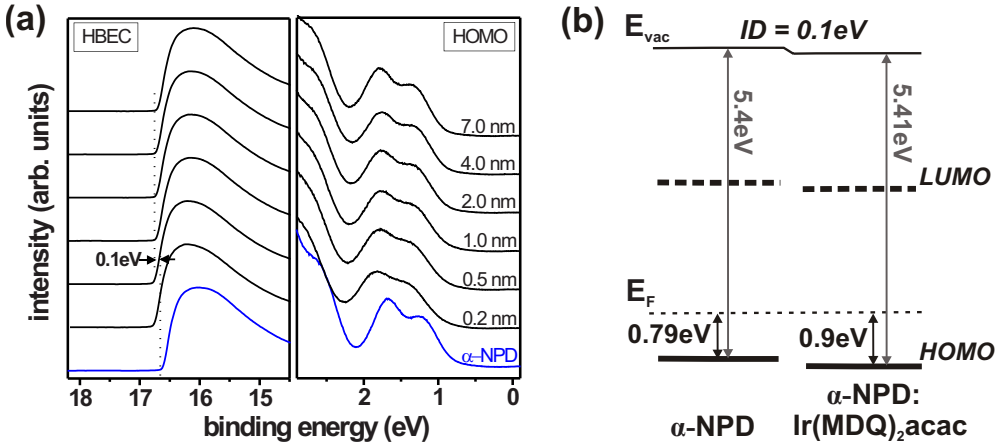

FIG. 4. (Color online) Interface between α-NPD and α-NPD coevaporated with 10 wt % $Ir(MDQ)_2acac$. (a) Development of the HBEC and HOMO region of the UPS He I spectra as a function of increasing thickness of the coevaporated layer. The dotted vertical line marks the change in the position of the HBEC. (b) Resulting schematic energy level diagram.

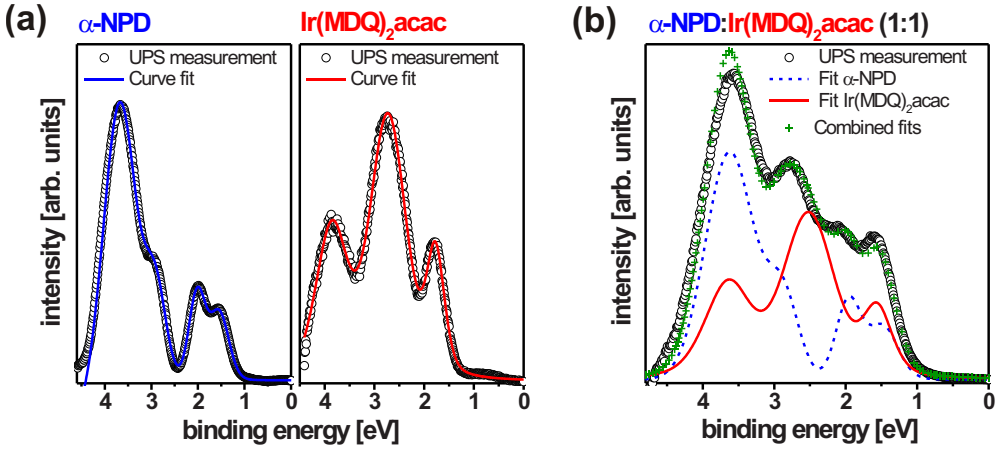

FIG. 5. (Color online) (a) UPS HOMO regions of pure α-NPD and pure $Ir(MDQ)_2acac$; the two measured curves are fitted by multiple Gaussian peaks after a polynomial background is subtracted. (b) UPS HOMO region of a 1:1 ratio of α-NPD mixed with $Ir(MDQ)_2acac$ after a polynomial background is subtracted; here the fitted curves from the pure layers are used to match the measured data.

is investigated. Again the doped MeO-TPD (6 nm) and intrinsic α-NPD (3 nm) are prepared on a silver sample. On top of that, the mixed layer of α-NPD:$Ir(MDQ)_2acac$ is deposited stepwise. The measurements in Fig. 4 show a small downward shift of the vacuum level and α-NPD HOMO position in the beginning by −100 meV that saturates after 1 nm when approximately one monolayer (ML) is closed. The HIB of the mixed layer is 0.9 eV and the IP remains the same as for intrinsic α-NPD.

Since the electron transport in the device takes place in the LUMO of the $Ir(MDQ)_2acac$ and not on the host material,[10] it is important to know the position of the $Ir(MDQ)_2acac$ HOMO and LUMO within the α-NPD matrix. The 10 wt % doping ratio used before does not produce distinct HOMO features from the iridium complex molecules. Therefore two more samples were prepared, one with a doping ratio α-NPD:$Ir(MDQ)_2acac$ of 1:1 and a pure $Ir(MDQ)_2acac$ sample. In Fig. 5(a), the HOMO region of the

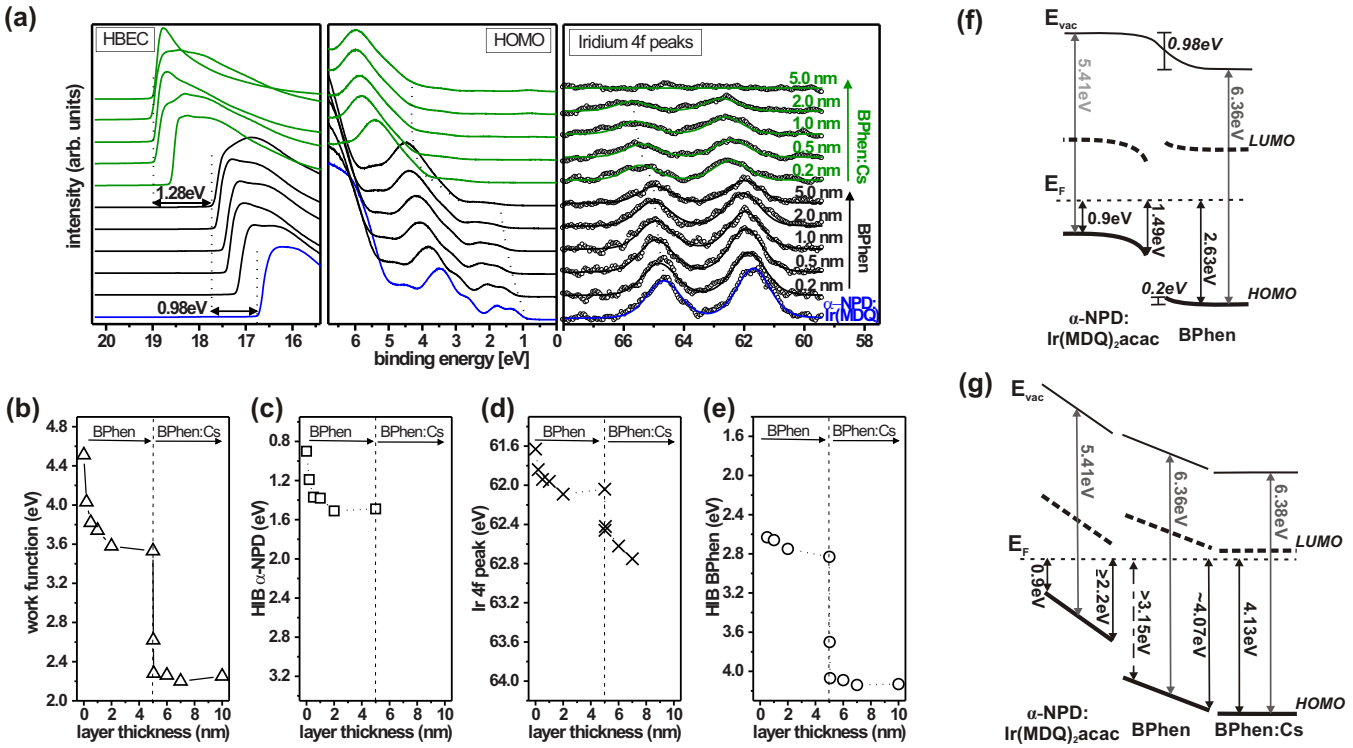

FIG. 6. (Color online) Interface from α-NPD:$Ir(MDQ)_2acac$ to BPhen and to BPhen:Cs. (a) Development of the HBEC and HOMO region of the UPS He I spectra and Ir 4*f* XPS peaks with increasing thickness of the organic layers; the dotted vertical lines mark the change in the position of the HBEC, HOMO, and Ir $4f_{7/2}$ peak. Change in (b) work function, (c) α-NPD HIB, (d) Ir $4f_{7/2}$ peak, and (e) BPhen HIB as a function of the increasing BPhen and BPhen:Cs layer thickness; the dashed vertical line marks the start of the doped BPhen layer. (f) Resulting schematic energy level diagram for BPhen deposited on α-NPD:$Ir(MDQ)_2acac$. (g) Resulting schematic energy level diagram when BPhen:Cs is deposited on α-NPD:$Ir(MDQ)_2acac$/BPhen.

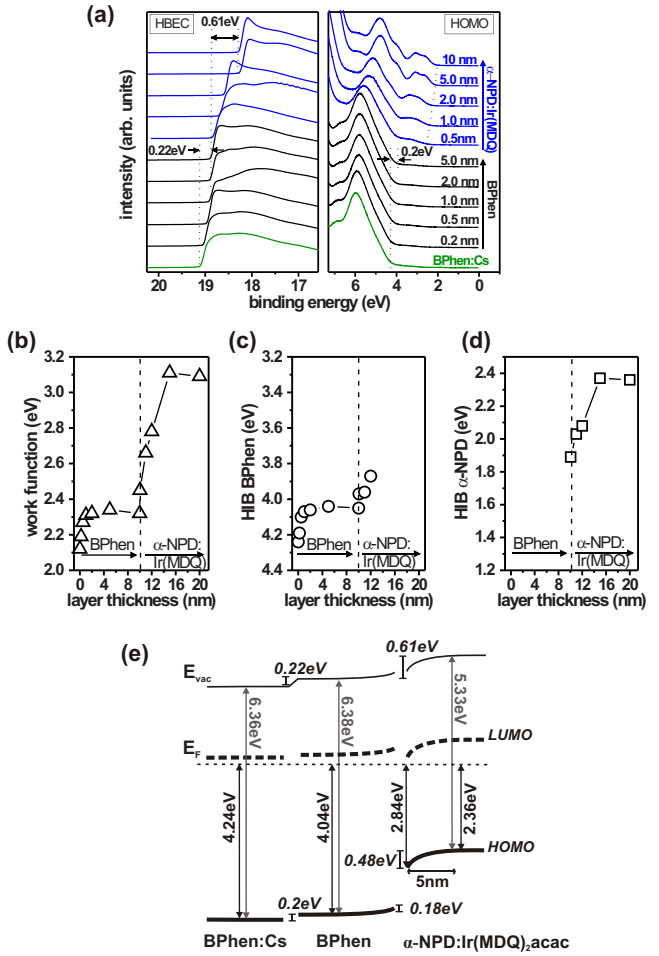

FIG. 7. (Color online) Interface from BPhen:Cs to BPhen and to α-NPD:Ir$(MDQ)_2$acac. (a) Development of the HBEC and HOMO region of the UPS He I spectra with increasing thickness of the organic layers. Change in (b) work function, (c) BPhen HIB, and (d) α-NPD HIB as a function of the BPhen and α-NPD:Ir$(MDQ)_2$acac layer thickness; the dashed vertical line marks the start of the α-NPD:Ir$(MDQ)_2$acac layer. (e) Resulting schematic energy level diagram.

pure α-NPD layer and the pure Ir$(MDQ)_2$acac layer are shown, fitted by multiple Gaussian peaks after a polynomial background is subtracted. These two fits are used in the HOMO region of the 1:1 mixed layer [Fig. 5(b)] and are shifted in relative position and intensity to match the measured data. This fit shows that the HOMO cutoffs are at the same position, so the HOMO of the α-NPD and the iridium complex molecule are aligned in the mixed layer. The position of the Ir$(MDQ)_2$acac LUMO can be estimated from the 2.6 ± 0.2 eV transport gap measured by cyclic voltammetry to be 0.5 eV below the LUMO of α-NPD.

For the investigation of the interface between α-NPD:Ir$(MDQ)_2$acac and the hole-blocking layer BPhen, a silver foil with doped MeO-TPD (5 nm) and α-NPD:Ir$(MDQ)_2$acac (5 nm) is prepared. Here the intrinsic α-NPD had to be left out to prevent a charging of the sample during measurement by the photogenerated holes. This has no effect on the alignment since it does not lead to a change in the energetic position of the mixed layer, as can be seen in the same HIB of α-NPD:Ir$(MDQ)_2$acac in Figs. 4(b) and 6(f). The UPS measurements in Fig. 6(a) and the resulting values in Fig. 6(c) show that upon BPhen deposition, the HOMO of α-NPD:Ir$(MDQ)_2$acac exhibits a downward shift by −590 meV; therefore the HIB of this layer increases to 1.49 eV. The HOMO of BPhen can be distinguished after 0.5 nm of coverage; for increasing thickness, it shows a downward bending of −200 meV [Fig. 6(e)]. The energetic alignment of this interface is shown in Fig. 6(f). The strong vacuum-level shift when depositing an intrinsic layer is unusual and must be the result of a chemical reaction between the dissociated $Ir(MDQ)_2^+$ fragments and BPhen molecules at the interface creating a dipole layer.[10]

Since UPS has only a small probing depth, the change in position of the iridium $4f$ core-level peaks is observed by XPS as well [right side of Fig. 6(a)], which yields additional information on the behavior of the mixed layer. These core-level peaks show a downward shift by −410 meV in Fig. 6(d), following the UPS shift in shape but not in intensity. This can have two different reasons: (i) XPS probes deeper into the sample, so the bending of a lower layer is observed or (ii) the reaction between the iridium complex molecules and BPhen at the interface could induce a different energy shift of the α-NPD compared to the Ir$(MDQ)_2$acac.

A total BPhen thickness of only 5 nm is chosen since on the same sample, the measurement is continued with the electron-injection layer of BPhen doped with cesium atoms. A thicker intrinsic BPhen layer would increase the probability of charging during the following measurement. Instantaneously after the deposition of 2 Å of doped BPhen, the work function changes by −900 meV and the BPhen HOMO moves downward by −920 meV as can be seen at the dotted vertical line in Figs. 6(b) and 6(e). Since at such low coverage, the HOMO signal originates mostly from the underlying intrinsic BPhen, this must mean that at the interface, the energy levels of the intrinsic BPhen layer shift downward to achieve alignment with the doped BPhen. Upon further deposition, the vacuum level moves downward even more, resulting in a total shift of −1.28 eV while the HOMO shows a total shift of −1.3 eV. The doping ratio can be estimated from the relative carbon and cesium XPS peak intensities and accounts in this case for one cesium atom per BPhen molecule.

In this measurement the HOMO position of the underlying α-NPD:Ir$(MDQ)_2$acac layer cannot be distinguished anymore. However, by following the XPS iridium peak shift, the influence of the n-doped layer can still be observed. Upon BPhen:Cs deposition, a sudden downward shift of −420 meV occurs in the Ir peak position as shown in Fig. 6(d); for a BPhen:Cs thickness of 2 nm, this value further increases to −710 meV without showing saturation. It is thus most likely the shifting continues but for thicker BPhen:Cs layers, the XPS signal becomes too faint to be detectable as well. If one assumes a similar shift of the iridium XPS peak and HOMO of α-NPD, then the HIB should have increased to at least 2.2 eV due to the contact with the n-doped layer. In Fig. 6(g), the assumed band alignment from this measurement is shown. The position of the HOMO of BPhen at the interface to α-NPD:Ir$(MDQ)_2$acac cannot be derived from the measurement since it will move downward by some un-

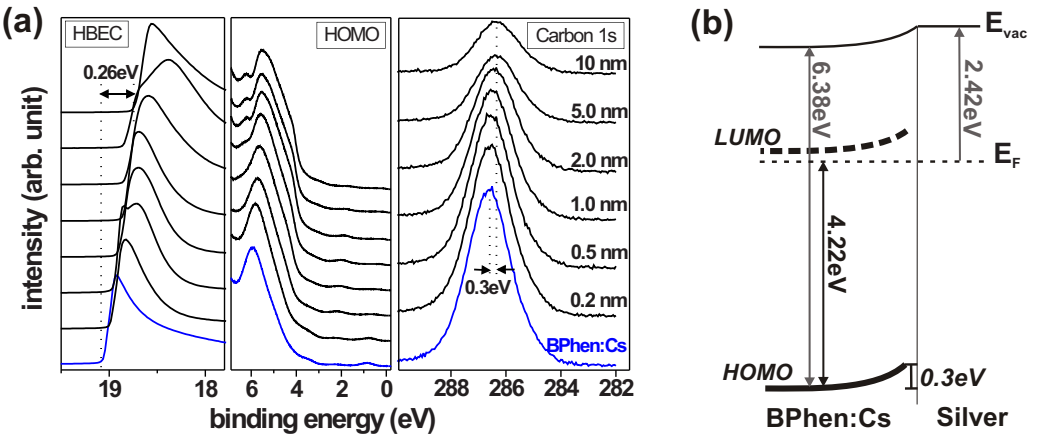

FIG. 8. (Color online) Interface from BPhen:Cs to silver. (a) Development of the HBEC and HOMO region of the UPS He I spectra and C 1*s* XPS peak with increasing thickness of the metal top contact; the dotted vertical lines mark the change in the position of the HBEC and C 1*s* peak. (b) Resulting schematic energy level diagram.

known amount. A minimum HIB of 3.15 eV can be assumed since otherwise an upward dipole from the mixed layer would result. In the schematic energy diagrams of Fig. 6, a transport gap of 4.4 ± 0.2 eV is assumed for BPhen; this is concluded from the UPS measurement of the doped BPhen layer since here the LUMO is positioned close to the Fermi energy.

More measurements are needed to determine the HOMO position of the intrinsic BPhen at the contact to α-NPD:$Ir(MDQ)_2$acac and to learn more about the alignment between BPhen and BPhen:Cs. Therefore, the reversed deposition sequence is investigated as well and is shown in Fig. 7(a). BPhen:Cs of 10 nm is deposited on a silver foil, followed by a stepwise deposition of 10 nm BPhen. The measured values in Fig. 7(c) reveal a small interface dipole of approximately 200 meV that is created within the first ML when the HIB changes from 4.24 eV for the doped layer to 4.04 eV for the intrinsic one. The schematic alignment is shown on the left part of Fig. 7(e). On top of this layer, α-NPD:$Ir(MDQ)_2$acac is evaporated. The HOMO of BPhen gradually shifts upward by 180 meV upon the deposition of the mixed layer and α-NPD:$Ir(MDQ)_2$acac shows a shift of 480 meV as can be seen in Fig. 7(d) starting from the dashed line. Since the BPhen layer shows only a small change in energetic position here, the backward measurement demonstrates that most of the shifting seen in the forward measurement (Fig. 6) occurs in the mixed layer.

It would be interesting to know how the layers behave when *p*-MeO-TPD is evaporated on top. This should pull the HOMO of the mixed layer up to a HIB of 0.9 eV again and might influence the energetic position of the intrinsic BPhen. However, it was not possible to do this measurement as the sample shows immediate charging. From the combined measurements in forward and backward directions, the actual energy alignment of these interfaces is derived and is shown as a part of Fig. 9. As stated before, we cannot exclude that the intrinsic BPhen layer would be shifted further by the built-in potential created between the two doped layers. The same holds true for the intrinsic α-NPD layer that could not be included in the stack for most of the measurements; some of the built-in potential could drop across this layer.

As a last step, the interface to the silver top contact is investigated. For that purpose, 15 nm of BPhen:Cs is evaporated on a silver foil and afterward silver is stepwise deposited on top. The shift of the HOMO of BPhen is difficult to distinguish in the UPS spectra [Fig. 8(a)] since the silver 4*d* levels are located around the same binding energy. From the change in the position of the XPS carbon 1*s* state, we can derive that the organic shifts upward by 300 meV. The position of the vacuum level changes by about 260 meV when 10 nm silver is evaporated on top, which results in a work function of 2.4 eV that differs from the value for bulk silver. This effect is well known for metal top contacts on organics[15,16] and is probably due to the fact that one monolayer of the organic material remains on top of the metal layer. Therefore, it is assumed in Fig. 9 that the silver top contact has a work function of 4.3 eV even though it is not observable by UPS because of the residual BPhen on top. The thickness of the depletion layer cannot be derived from this measurement. However, by changing the deposition sequence in a separate experiment and evaporating BPhen:Cs stepwise on silver, it is determined to be in the range of 3 nm.

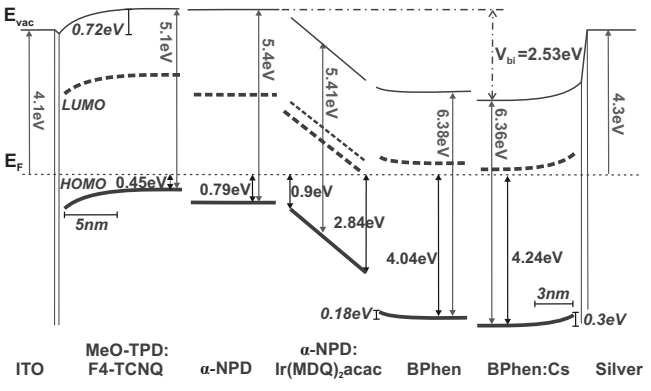

FIG. 9. Schematic energy diagram of the full OLED device as it can be derived from the measurements presented in this paper. The LUMO of the α-NPD is shown only as a thin line since the electron transport happens on the LUMO of the $Ir(MDQ)_2$acac. The built-in potential V_{bi} is calculated from the offset between the vacuum levels of the doped layers.

In Fig. 9 the full alignment of the red phosphorescent OLED stack is shown. Due to the induced large carrier concentration on the order of 10^{18} cm^{-3}, the doping shifts the HOMO of the *p*-type layer and LUMO of the *n*-type layer close to the Fermi energy, creating a depletion layer at the interface to the metal contact. This improves the charge-carrier injection since the electrons and holes can efficiently tunnel through the narrow depletion region. In addition the conductivity increases by several orders of magnitude.[17] This position close to the Fermi energy is only determined by the host material and the amount of doping but is independent of the choice of metals used as contacts. Therefore the doped layers decouple the organic stack from the metals and the performance is mainly determined by the built-in voltage created by the doped layers and not by the difference in the metal work functions. The choice of metal will still have some influence since it will affect the width and bending direction of the depletion layer.

To relate this measured built-in voltage to the performance of an OLED device, the current-voltage characteristics of the investigated stack are shown in Fig. 10. Four samples are compared where the width of the emission layer α-NPD:Ir(MDQ)$_2$acac is varied between 5 and 20 nm. The current characteristic can be divided into three regions. For voltages below 2 V, the leakage currents dominate. In the range from 2 V to approximately the built-in voltage of 2.5 V, all curves coincide and in this regime the shape can be explained by the ideal-diode equation for *p-n* junctions considering the drift-diffusion regions. Above this voltage, the current gets dominated by recombination and/or Ohmic conduction and the curves show a significant dependence on the thickness of the emission layer which indicates a considerable drop of bias across this region.

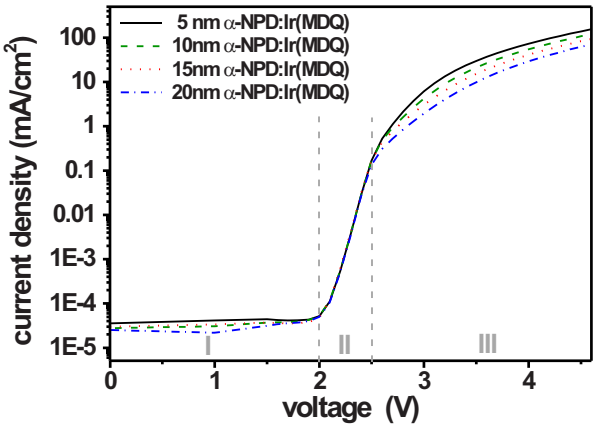

FIG. 10. (Color online) Current-voltage characteristic of the red phosphorescent OLED stack at different thicknesses of the emitting layer α-NPD:Ir(MDQ)$_2$acac. The current can be divided intro three regions: (I) leakage-current, (II) drift-diffusion-dominated, and (III) recombination/Ohmic-conduction-dominated region.

IV. SUMMARY

In conclusion, based on UPS and XPS measurements, we present the full energetic alignment of an OLED as it is summarized in Fig. 9. The data prove that there is no common vacuum level throughout the device. This is mainly due to the interface dipoles at the contacts and the properties of the doped layers. The adjacent intrinsic layers show nearly vacuum-level alignment, with only small deviations due to interface dipoles. In the doped layers, one can furthermore observe the typical level-bending effects and the small distance between transport level and Fermi energy. The *p* and *n* doping of the injection layers leads to a built-in voltage of 2.53 V in this device which mainly drops across the α-NPD:Ir(MDQ)$_2$acac layer.

ACKNOWLEDGMENT

This work was funded by the German BMBF under Contract No. 13N 8855, project acronym "ROLLEX."

*olthof@iapp.de
†www.iapp.de

[1] K. Walzer, B. Maennig, M. Pfeiffer, and K. Leo, Chem. Rev. (Washington D.C.) **107**, 1233 (2007).
[2] H. Ishii, K. Sugiyama, E. Ito, and K. Seki, Adv. Mater. **11**, 605 (1999).
[3] J. Blochwitz, T. Fritz, M. Pfeiffer, K. Leo, D. M. Alloway, P. A. Lee, and N. R. Armstrong, Org. Electron. **2**, 97 (2001).
[4] I. G. Hill, D. Milliron, J. Schwartz, and A. Kahn, Appl. Surf. Sci. **166**, 354 (2000).
[5] J. X. Tang, C. S. Lee, and S. T. Lee, J. Appl. Phys. **101**, 064504 (2007).
[6] A. Kahn, N. Koch, and W. Gao, J. Polym. Sci., Part B: Polym. Phys. **41**, 2529 (2003).
[7] J. X. Tang, K. M. Lau, C. S. Lee, and S. T. Lee, Appl. Phys. Lett. **88**, 232103 (2006).
[8] S. Braun, M. P. de Jong, W. Osikowicz, and W. R. Salaneck, Appl. Phys. Lett. **91**, 202108 (2007).
[9] I. Salzmann, S. Duhm, G. Heimel, M. Oehzelt, R. Kniprath, R. L. Johnson, J. P. Rabe, and N. Koch, J. Am. Chem. Soc. **130**, 12870 (2008).
[10] R. Meerheim, S. Scholz, S. Olthof, G. Schwartz, S. Reineke, K. Walzer, and K. Leo, J. Appl. Phys. **104**, 014510 (2008).
[11] R. Schlaf, H. Murata, and Z. H. Kafafi, J. Electron Spectrosc. Relat. Phenom. **120**, 149 (2001).
[12] G. He, K. Walzer, M. Pfeiffer, K. Leo, R. Pudzich, and J. Salbeck, Proc. SPIE **5519**, 42 (2004).
[13] S. Krause, M. B. Casu, A. Schöll, and E. Umbach, New J. Phys. **10**, 085001 (2008).
[14] S. Duhm, G. Heimel, I. Salzmann, H. Glowatzki, R. L. Johnson, A. Vollmer, J. P. Rabe, and N. Koch, Nature Mater. **7**, 326 (2008).
[15] B. Jaeckel, J. B. Sambur, and B. A. Parkinson, Langmuir **23**, 11366 (2007).
[16] I. G. Hill, A. Rajagopal, and A. Kahn, J. Appl. Phys. **84**, 3236 (1998).
[17] M. Pfeiffer, K. Leo, X. Zhou, J. S. Huang, M. Hofmann, A. Werner, and J. Blochwitz-Nimroth, Org. Electron. **4**, 89 (2003).